

# Apprehending ganglioside diversity: a comprehensive methodological approach<sup>S</sup>

Elodie A. Y. Masson,<sup>1,\*†,§</sup> Estelle Sibille,<sup>\*,†,§</sup> Lucy Martine,<sup>\*,†,§</sup> Fanny Chaux-Picquet,<sup>\*\*,†</sup>  
Lionel Bretillon,<sup>\*,†,§</sup> and Olivier Berdeaux<sup>\*,†,§</sup>

CNRS,\* UMR6265 Centre des Sciences du Goût et de l'Alimentation, F-21000 Dijon, France; INRA,<sup>†</sup> UMR1324 Centre des Sciences du Goût et de l'Alimentation, F-21000 Dijon, France; Université de Bourgogne Franche-Comté,<sup>§</sup> UMR Centre des Sciences du Goût et de l'Alimentation, F-21000 Dijon, France; and Institut de Chimie Moléculaire de l'Université de Bourgogne,<sup>\*\*</sup> UMR 6302 CNRS, Université de Bourgogne Franche-Comté, F-21000 Dijon, France

**Abstract** Gangliosides (GGs) make a wide family of glycosphingolipids ubiquitously expressed in mammalian tissues and particularly abundant in the brain and nervous system. They exhibit a huge diversity due to structural variations in both their oligosaccharidic chain and ceramide moiety, which represent a real analytical challenge. Since their discovery in the 1940s, methods have persistently improved until the emergence of LC/MS, which offers a high level of specificity and sensitivity and is suitable with high-throughput profiling studies. We describe here a comprehensive approach relying on various techniques and aiming at fully characterizing GGs in biological samples. First, total GG content was determined by a biochemical assay. Second, GG class composition was assessed by high-performance thin-layer chromatography followed by colorimetric revelation. Then, ceramide types of GG classes were identified, and their relative quantification was performed thanks to the development of a powerful and reliable LC/MS method. Finally, ceramides were structurally characterized, and minor and less common GG classes were identified using high-resolution MS. These methods were applied to the rat retina to provide an exhaustive description of its GG composition, giving the base for a better understanding of the precise roles of GGs in this tissue.—Masson, E. A. Y., E. Sibille, L. Martine, F. Chaux-Picquet, L. Bretillon, and O. Berdeaux. Apprehending ganglioside diversity: a comprehensive methodological approach. *J. Lipid Res.* 2015. 56: 1821–1835.

**Supplementary key words** glycosphingolipids • liquid chromatography • molecular species • retina

Gangliosides (GGs) make an extremely wide and heterogeneous family of glycosphingolipids. They are amphiphatic molecules composed of a hydrophobic ceramide moiety on which a hydrophilic oligosaccharidic chain is

branched (Fig. 1A). The presence of one or more sialic acids in this chain makes the distinctive feature of GGs. Since their first definition by Klenk in 1942 after their isolation from brain tissue and ganglion cells (1), almost 200 GGs have been described, presenting with differences in the structure, number, order, and linkage of the sugar residues (2). The structural complexity and diversity of GGs is reinforced by the variability of the ceramide moiety, depending on the length, saturation, and hydroxylation of both the long chain base (LCB) and the FA. GGs result from the sequential glycosylations and sialylations of the ceramide precursor, as illustrated in the biosynthetic scheme presented in Fig. 1B. The distribution pattern of these GG classes is specific to the tissue, cell type, differentiation, or developmental stage (3). GGs are present primarily in the outer leaflet of the plasma membrane and are assumed to be concentrated in ordered microdomains referred to as lipid rafts [for reviews on the concept, see (4–7)]. Their bifunctional role is directly linked to this special localization. First, they are implicated in cell matrices and cell-cell recognition events. They are receptors for microorganisms, and their toxins and also interact with other glycosphingolipids, counterpart lectins, and adhesion receptors such as integrins. Second, they modulate transmembrane signaling, mainly by interacting with growth factor receptor-associated protein kinases. Through these functions, GGs can regulate cell proliferation and apoptosis, adhesion, migration, and differentiation (8).

Abbreviations: ACN, acetonitrile; CHCl<sub>3</sub>, chloroform; CH<sub>3</sub>OH, methanol; CID, collision-induced dissociation; GG, ganglioside; GD, disialoGG; GM, monosialoGG; GG-NANA, GG-bound sialic acid; GP, pentasialoGG; GQ, quadrisialoGG; GT, trisialoGG; HILIC, hydrophilic interaction liquid chromatography; HPTLC, high-performance thin-layer chromatography; HRMS, high-resolution mass spectrometry; LCB, long chain base; NANA, N-acetylneuraminic acid; QqQ, triple quadrupole; SRM, selected reaction monitoring.

<sup>†</sup>To whom correspondence should be addressed.

e-mail: elodie.masson@dijon.inra.fr

<sup>S</sup> The online version of this article (available at <http://www.jlr.org>) contains a supplement.

This work was supported by the French National Institute for Agricultural Research (INRA), the Regional Council of Burgundy (France), and the FEDER (European Funding for Regional Economic Development).

Manuscript received 18 May 2015 and in revised form 30 June 2015.

Published, JLR Papers in Press, July 4, 2015

DOI 10.1194/jlr.D060764

Copyright © 2015 by the American Society for Biochemistry and Molecular Biology, Inc.

This article is available online at <http://www.jlr.org>

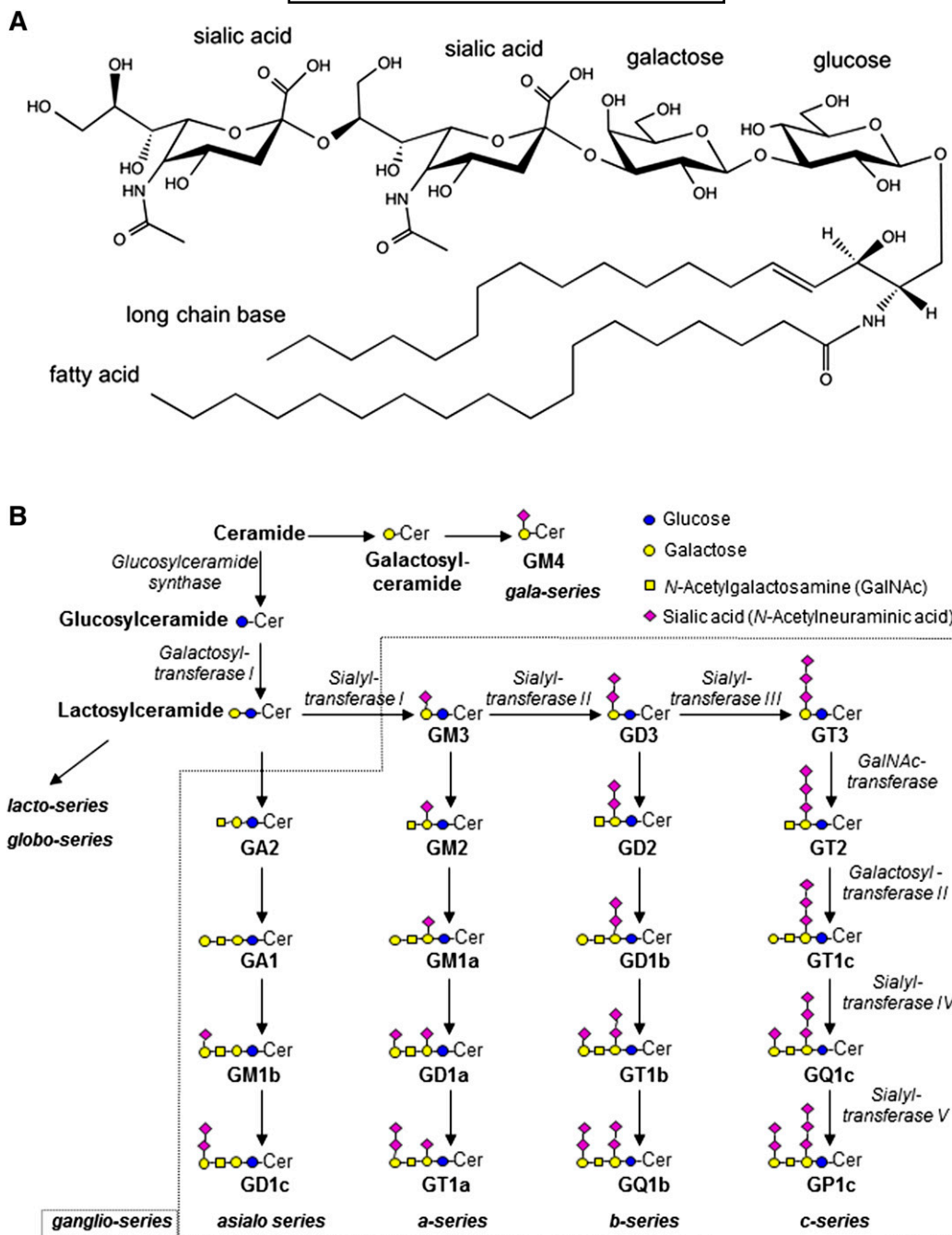


**Fig. 1.** Structure of a GG and general scheme of biosynthesis. A: GGs are made of a ceramide moiety composed of a long chain base (LCB) and a FA whose alkyl chains may vary, and on which a sugar chain is branched. GD3 34:1 (based on LIPID MAPS, systematic name: NeuAc $\alpha$ 2-8NeuAc $\alpha$ 2-3Gal $\beta$ 1-4Glc $\beta$ -Cer) is given as an example. Ceramide is composed of sphingosine (d18:1) as LCB and stearic acid (18:0) as FA. The oligosaccharidic chain is made of one glucose, one galactose, and two sialic acid residues, characteristic of GGs. B: The formation of GGs is catalyzed by the sequential action of glycosyltransferases (italic). The main GG classes of the ganglio-series, the most widely expressed and sharing the common core structure Gal $\beta$ 3GalNAc $\beta$ 4Gal $\beta$ 4Glc, are represented with their common names, according to Svennerholm (49). GD, disialoGG; GM, monosialoGG; GP, pentasialoGG; GQ, quadrisialoGG; GT, trisialoGG. The symbol nomenclature is according to Schnaar et al. (50).

Although GGs are ubiquitously expressed in mammalian tissues, they are particularly abundant in the brain and nervous tissues. The role of GGs in the nervous system has been extensively investigated, and their importance is now well established (9). In vitro, GGs have been associated with

neuritogenesis, survival, and adhesion of neural cells (8). In vivo, expression levels of GGs undergoes dramatic changes during brain development, characterized by an increase of complex GGs (i.e., with longer polysaccharidic chains). In recent years, the phenotype of a number of knockout mice

for GG synthase genes has been characterized. These models present with varying degrees of neurological disorders generally aggravating with age: motor and sensory dysfunctions, hyperactivity, impaired nerve regeneration, demyelination, and inflammation in neurons (10–12). In humans, dysregulations of GG metabolism characterized by GG accumulation into lysosomes cause severe neurodegenerative diseases, such as Tay-Sachs or Sandhoff diseases (13). An epilepsy syndrome among the Amish people has also been found to be associated with a GM3 synthase deficiency (14). GG also seem to be of importance in the retina, a neural tissue that is a direct extension of the central nervous system. Indeed, GG composition of the retina undergoes drastic changes during the development of the tissue, concomitantly to morphologic differentiation (15). Mouse models of GM2 gangliosidosis exhibit retinal abnormalities with visual deficiency (16, 17). Moreover, GM1 injections into the vitreous can protect the retina from lesions induced by ischemia (18) or optic nerve axotomy (19).

Efficient analytical methods are both a challenge and a requirement to apprehend and decipher the huge variability of GGs, as well as progress in the understanding of their various biological functions.

Until recently, GGs have been analyzed by high-performance thin-layer chromatography (HPTLC) coupled to densitometric detection after colorimetric revelation of sialic acids with resorcinol-HCl. Although this technique is easy to implement and gives an overview of the GG pattern of a biological sample, its low sensitivity and resolution are not really compatible with the subtleties that make GG heterogeneity. HPLC techniques were also developed, coupled to UV (20) or fluorimetric detection (21). Even though these techniques offer a better sensitivity than the previous one, they do not permit us to investigate the structure of the molecules. The need for more refined methods led to the development of MS approaches [for a review, see (22, 23)]. Indeed, identification of the molecules based on their exact mass offers a high level of precision and specificity. Usually, this identification is conveniently based on the detection of a characteristic fragment ion at  $m/z$  290 that corresponds to *N*-acetylneuraminic acid (NANA; sialic acid), common to every GG. New soft ESI methods especially appropriate for labile molecules such as GGs have been implemented. Although MS can be used with direct infusion of the extract, a prior LC separation step is often performed to achieve better analytical specificity and sensitivity, which stands at the femtomol level. These improvements have enabled us to study GGs in tissues where they are not as abundant as in nervous tissues (plasma, milk, and various cell types). Tandem ESI/MS also allows for quantification provided that appropriate internal standards are used to normalize for differences in ionization and fragmentation of molecular species. Moreover, high-resolution and high-mass accuracy of some mass analyzers enable effective molecular structure elucidation, which, in the past, relied on cumbersome comprehensive chemical analyses. Higher precision in the analysis has offered the possibility to elucidate oligosaccharidic chains and thus identify novel GG molecules of

potential importance. It has also allowed characterizing the ceramide moiety of GG, whose heterogeneity significance is still largely unknown. Finally, the relatively high-throughput capabilities of MS have enabled the emergence of “omic” approaches in the field of glycosphingolipids, giving access to the diversity of molecular species of GGs (24).

This study offers a comprehensive and progressive approach to analyze GGs in a biological sample. First, total GG content was assessed with the biochemical resorcinol assay, and GG class pattern was determined by HPTLC coupled to colorimetric revelation. Then, LC/MS enabled the determination of the various ceramide types represented in each GG class and their relative quantification. Finally, ceramide types were structurally characterized, and minor GG classes identified thanks to high-resolution MS (HRMS). We applied these methods to the rat retina and thus provided an exhaustive description of the diversity of GG molecular species in this tissue, prerequisite for a better understanding of the precise roles of GGs in the retina.

## MATERIALS AND METHODS

### Materials

Chloroform ( $\text{CHCl}_3$ ) and methanol ( $\text{CH}_3\text{OH}$ ) were obtained from SDS (France). Ammonium acetate, acetonitrile (ACN),  $\text{CH}_3\text{OH}$ , and water of Optima LC/MS grade were all from Fisher Scientific (France). Commercially available GG standards from natural sources (bovine or human) were obtained from Matreya LLC.

### Retina sample preparation

Retinas were dissected from 3-month-old Wistar rats. Pairs of retina were weighed and thoroughly homogenized in 0.3 ml distilled water with tungsten microbeads using a tissue lyser (Qia-gen, The Netherlands; 1 min, 30 s at 30 Hz speed). A 40  $\mu\text{l}$  aliquot of each sample was used to measure protein content. The rest of the sample was adjusted to 0.5 ml water and used for GG extraction. Investigations were conducted in conformity with the Public Health Service policy on use of laboratory animals and were approved by a local ethics committee (Comité d’Ethique de l’Expérimentation Animale C2EA, Dijon, France).

### Quantitative determination of protein content

The 40  $\mu\text{l}$  aliquot of retina homogenate was lysed by adding 10  $\mu\text{l}$  of 5 $\times$  Ripa buffer, on ice for 30 min. After clearing by centrifugation (10,000  $g$ , 10 min, 4°C), total protein content was measured on the supernatant using the BCA method (BCA protein assay kit according to manufacturer’s instructions; Pierce Biotechnology, Thermo Scientific) with BSA as a standard (Sigma-Aldrich).

### Extraction, separation, and purification of GGs

First, total lipids were extracted from the samples dissolved in 0.5 ml water, overnight at 4°C, with 10 vol (5 ml) of  $\text{CHCl}_3/\text{CH}_3\text{OH}$  (1:1, v/v). The residual pellet obtained after centrifugation (1,500  $g$ , 5 min) was reextracted twice with 2 ml of the same solvent. The three lipid extracts were combined, dried under a stream of nitrogen, and redissolved in 3 ml  $\text{CHCl}_3/\text{CH}_3\text{OH}$  (1:1, v/v). Second, GGs were separated from other lipids by phase

partition by adding 1 ml water. After centrifugation, the upper aqueous phase was collected while the lower organic phase was reextracted twice with 2 ml CH<sub>3</sub>OH/water (1:1, v/v). The three upper phases containing GGs were combined, dried under a stream of nitrogen, and redissolved in 2 ml CH<sub>3</sub>OH/PBS 10 mM (1:1, v/v). Third, this GG extract was desalted on a C18 silica gel column (Sep-Pak Vac 6cc, 500 mg; Waters) washed with 7 ml CH<sub>3</sub>OH and preequilibrated with 7 ml CH<sub>3</sub>OH/PBS 10 mM (1:1, v/v). After washing with 10 ml water, purified GGs were eluted with 6 ml CH<sub>3</sub>OH and 4 ml CHCl<sub>3</sub>/CH<sub>3</sub>OH (2:1, v/v). GGs obtained from the retinas of four rats were pooled in CHCl<sub>3</sub>/CH<sub>3</sub>OH (2:1, v/v) and stored, under nitrogen, at -20°C until further analyses.

### Quantitative determination of GG-bound sialic acid content

GG-bound sialic acid (GG-NANA) was measured on purified GG extracts, using the procedure of Svennerholm with slight modifications (25). Commercial sialic acid (NANA; Sigma-Aldrich) was used as a standard for the assay. Standards (0–30 nmol NANA) or aliquots of GG extracts (equivalent to 3.5 retinas) were first dissolved in 0.25 ml distilled water and placed to react with 0.25 ml of resorcinol reagent at 110°C for 20 min in a water bath. The resorcinol reagent was prepared as follows: 10 ml resorcinol 2% (Sigma-Aldrich), 40 ml hydrochloric acid, and 0.125 ml 0.1 M copper sulfate. After cooling in ice, 0.75 ml butyl acetate-1-butanol (85:15, v/v) was added to the tubes in order to extract the purple-blue color resulting from the reaction of sialic acids with the resorcinol reagent. The upper solvent phase was collected after centrifugation (1,500 g, 3 min). Optical density was finally read at 580 nm in a spectrophotometer.

### GG analysis by HPTLC

Aliquots of the GG extracts (equivalent to 2.5 retinas) were applied to an HPTLC plate (Merck, Germany). The plate was developed in CHCl<sub>3</sub>/CH<sub>3</sub>OH/0.2% CaCl<sub>2</sub> (55:45:10, v/v/v) for 45 min, sprayed with resorcinol reagent, and covered with a clean glass plate to be heated at 120°C for 20 min. GGs, appearing as purple-blue bands, were identified by comigration with standards. A standard curve was also performed for each GG class by spotting increasing known amounts of GG standards on an HPTLC plate. A densitometric analysis of the GG-bound sialic acid detected on the plates was performed, using a charge-coupled device (CCD) camera (Chemidoc<sup>TM</sup> MP System; Biorad). Retina GGs were then quantified using the standard curves established for each GG class.

### GG analysis by LC/MS

**HPLC.** LC was performed using a Dionex UltiMate<sup>TM</sup> 3000 LC pump from ThermoScientific equipped with an autosampler. Separation of GM3, GM2, GM1, GD3, GD1a, GD1b, GT1b, and GQ1b standards was achieved under hydrophilic interaction liquid chromatography (HILIC) conditions using a silica Kinetex column (150 mm × 2.1 mm inner diameter, 2.6 μm, HILIC; Phenomenex). The mobile phase consisted of (A) ACN/water (90:10, v/v) containing 10 mM ammonium acetate and (B)

ACN/water (50:50, v/v) containing 10 mM ammonium acetate. The solvent-gradient system was as follows: 0–1 min 100% A, 4 min 79% A, 9 min 78% A, 14–18 min 50% A, and 19–48 min 100% A. The flow rate was 400 μl min<sup>-1</sup>, the injection volume was 10 μl, and the column was maintained at 30°C.

**MS.** Eluate from the HPLC system was introduced alternatively in two different mass spectrometers: a TSQ Quantum Ultra triple quadrupole (QqQ) and a LTQ-Orbitrap XL<sup>TM</sup> (Thermo Scientific).

**TSQ Quantum Ultra.** The QqQ mass spectrometer was equipped with a heated electrospray (HESI-II) probe as the ionization source. The mass spectrometer was operated in negative ion mode and controlled by TSQ Tune version 1.5 software. Nitrogen was used for both the sheath and the auxiliary gases. The MS signals of GG species were first optimized in the MS full scan mode (range from 500 to 1,500 Da) by continuous infusion (10 μl min<sup>-1</sup>) of the standards (10 μg ml<sup>-1</sup>) dissolved in the mobile phase. The number of sialic acid residues present on a GG molecule determines the number of possible charge states that may be observed in its mass spectra. For each GG class, we used the charge state with the greatest intensity to compile our mass list. Thus, when operated in the single-stage MS negative ionization mode, monosialoganglioside molecular species produced abundant [M-H]<sup>-</sup> ions; GD3, GD1, and GT1b molecular species produced abundant [M-2H]<sup>2-</sup> ions; and GQ1b molecular species produced abundant [M-3H]<sup>3-</sup> ions. For each GG class, the main working parameters of the mass spectrometer are listed in **Table 1**.

For characterization, collision-induced dissociation (CID) of each deprotonated molecule was performed in the negative mode with argon as the collision gas at 1.5 mTorr. An abundant product ion at *m/z* 290 corresponding to a characteristic NANA fragment was obtained from [M-xH]<sup>x-</sup> ions of the different GG molecular species. This fragment was used for precursor ion scanning, whereby the [M-xH]<sup>x-</sup> ions of GG were specifically detected (signal/noise >3). For quantification, data were acquired in selected reaction monitoring (SRM) using Xcalibur 2.0.7 software (Thermo Scientific) from aliquots of GG extracts equivalent to a tenth of a retina. The precursor and product ion pairs for the SRM analysis were selected based on the precursor ion scanning, but some species were not considered in SRM because they stand below the quantification limit (signal/noise <10). Each sample was injected in triplicate. The proportion of each molecular species of a specific GG class was calculated as the ratio of its peak area to the sum of all detected peak areas in this class, every GG class being considered separately. The accuracy and repeatability of the method were evaluated by performing between-day and within-day precision using a GG standard mixture as well as a rat retina GG extract.

**Thermo LTQ-Orbitrap XL<sup>TM</sup>.** This hybrid mass spectrometer was used for high-resolution analyses. It was equipped with a heated electrospray (HESI-II) probe as the ionization source and

TABLE 1. QqQ mass spectrometer working parameters

GG	ESI Spray Voltage (kV)	Vaporizer Temperature (°C)	Sheath Gas (a.u.)	Auxiliary Gas (a.u.)	Sweep Gas (a.u.)	Capillary Temperature (°C)	Tube Lens (V)	Skimmer Offset (V)
GM3	4.0	300	20	20	5	300	-230	8
GM2	4.0	300	20	20	2	300	-230	8
GD3	4.0	300	30	10	1	300	-110	8
GD1a/b	4.0	300	20	15	2	300	-150	8
GT1b	4.0	300	30	15	1	300	-140	8
GQ1b	4.0	300	20	20	0	300	-110	8

two ion detectors, an independent linear ion trap detector and an Orbitrap detector, presenting high-resolution and high-mass accuracy. The instrument was operated in positive ion mode and controlled by Thermo Tune Plus version 2.5.5. Nitrogen was used for ion source gases. The MS signals of GGs were first optimized by continuous infusion ( $10 \mu\text{l min}^{-1}$ ) of the standards ( $10 \mu\text{g ml}^{-1}$ ) dissolved in the mobile phase. The conditions are listed in **Table 2**. All spectra were acquired in the mass range  $m/z$  200–2,600 and with the resolution set value 30,000 at  $m/z$  400. For MS/MS analyses, the precursor ions were selected within an isolation width of 10. Higher-energy collisional dissociation (HCD) and CID were both used, using respectively nitrogen and helium as collisional gases. Fragmentation involved an activation  $Q$  value of 0.250, an activation time of 30 ms, and a collision energy value between 30 and 50 eV.

## RESULTS

### Measurement of the GG-bound sialic acid content

GG-NANA content is frequently used as an estimate of the total GG content of a biological sample, the presence of sialic acid being a distinctive feature of GG among lipids. It was measured using colorimetry as described in Materials and Methods. Rat retinas contained an average of  $3.0 \pm 0.59 \mu\text{g GG-NANA/mg protein}$ , which was equivalent to  $9.7 \pm 1.91 \text{ nmol GG-NANA/mg protein}$  ( $n = 9$ , mean  $\pm$  SD). Those levels were in accordance with previously published data in different species (chicken, rat, calf, and pig), which stand between 5.9 and 9.7 nmol GG-NANA/mg protein (26–28). However, the colorimetric reaction of the sialic acid molecule with resorcinol seems to be partially dependent on the nature of the GG that carries it. Especially, it appeared that the intensity of the signal of a nanomole of sialic acid decreases with the complexity of the oligosaccharidic chain of the GG carrying it, the simplest GG GM3 giving the signal closest to free sialic acid (commercial NANA used as a standard for the assay; supplementary Fig. 1). As a consequence, the GG-NANA content of samples rich in complex GGs, such as nervous tissues, will be, to some extent, underestimated.

### Evaluation of the GG pattern by HPTLC

A diversity of GG classes exists depending on the number, nature, and sequence of the residues making the oligosaccharidic chain (Fig. 1B). GG classes of rat retina were separated by HPTLC and revealed with resorcinol reagent as illustrated in **Fig. 2A**. Based on comigration

with standards, rat retina appeared to contain mainly complex polysialylated GGs: GD3, GD1a, GD1b, GT1b, and GQ1b. Minor amounts of monosialogangliosides (GM3 and GM1) could also be detected, as well as an unidentified class running just above GD1b. The GG composition of rat retina was determined by densitometric analysis of the HPTLC plate thanks to calibration curves we established for each GG class (supplementary Fig. 2). The distributions estimated from the four pools of retinas tested were very similar. Results expressed as nmol GG/mg protein are shown in Fig. 2B. GD3, GD1b, and GT1b were found to be expressed in almost equal amounts (1.7, 1.7, and 1.5 nmol/mg protein, respectively), accounting for 27%, 27%, and 25% of the total nmol of GG detected, respectively. GD1a was present at 0.7 nmol/mg protein (12% of the total nmol of GG detected) and GQ1b at 0.6 nmol/mg protein (9% of the total nmol of GG detected).

### Determination of the ceramide composition of the different GG classes by LC/MS

In order to further characterize the GGs present in rat retina, an LC/MS method was developed. We chose to separate the GG classes using LC prior to the ESI/MS analysis and thus optimized a method of HILIC separation. This technique has been shown to be particularly suited to the separation of highly polar molecules, such as GGs (29, 30). In our study, ammonium acetate was added at 10 mM to the mobile phase system of ACN/water to enhance separation, resolution, and selectivity using a HILIC silica column. By optimizing the concentration of ammonium acetate, the flow rate and the use of a pertinent gradient, a good baseline separation of GM3, GM2, GD3, GD1a, GD1b, GT1b, and GQ1b classes was achieved in a short analysis time. Only GM1 coeluted with GD3, which could, however, be distinguished thanks to MS. A precursor ion scanning in the negative mode of the NANA at  $m/z$  290, a characteristic fragment of GG, was first performed using the QqQ mass spectrometer. Results obtained are illustrated in **Fig. 3** giving a representative total ion chromatogram of rat retina GGs. GGs corresponding to commercial standards were detected, confirming the identification previously made by HPTLC: GM3, GD3, GD1a, GD1b, GT1b, and GQ1b. A few additional minor peaks could also be detected in between major GG classes ( $\alpha$ ,  $\beta$ ,  $\gamma$ ,  $\delta$ , and  $\epsilon$ ). They did not correspond to commercial standards and required HRMS to be characterized (see Orbitrap results below). The precursor ion scanning also allowed for the detection of the different molecular species present in the

TABLE 2. LTQ-Orbitrap mass spectrometer working parameters

GG	ESI Spray Voltage (kV)	Vaporizer Temperature ( $^{\circ}\text{C}$ )	Sheath Gas (a.u.)	Auxiliary Gas (a.u.)	Sweep Gas (a.u.)	Capillary Temperature ( $^{\circ}\text{C}$ )	Tube Lens (V)
GM3	4	300	10	10	2	350	172
GM2	4	300	10	10	2	350	172
GM1	4	300	10	10	2	350	172
GD3	4	300	25	5	2	350	173
GD1a/b	4	300	25	5	2	350	159.5
GT1b	4	300	20	5	2	350	183.5
GQ1b	4	300	20	5	2	350	183.5

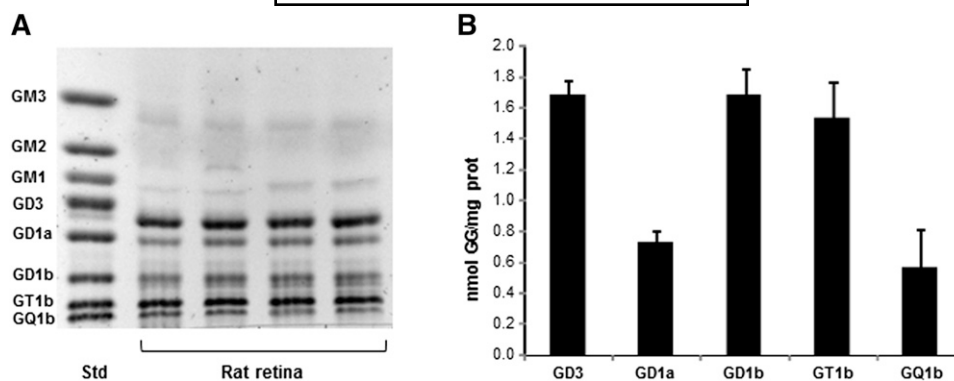


**Fig. 2.** GG profile of rat retina. A: Resorcinol-stained HPTLC plate of rat retina GGs. Std, standard mixture of GGs. 8.5 and 7 nmol GG-NANA were spotted for std and rat retina lanes, respectively. The plate was developed in  $\text{CHCl}_3/\text{CH}_3\text{OH}/0.2\% \text{CaCl}_2$  (55:45:10, v/v/v) and revealed with resorcinol reagent. B: Quantitative distribution of GG classes calculated from a standard curve of each GG class. Results are expressed in nmol GG/mg protein as mean  $\pm$  SD of four independent samples.

major GG classes. Indeed, each GG class exists in a number of molecular species, depending on the specific LCB and FA forming the ceramide moiety, which can both vary in length and number of unsaturations (Fig. 1A). The different species detected are listed in Table 3. GM3 and GD3 presented with the highest diversity (11 and 12 ceramide types, respectively), while the other GG classes were composed of 6 to 7 ceramide types. Ceramides ranged from 34 to 42 carbons, with one or two unsaturations. Ceramides 34:1, 36:2, 36:1, 38:2, 38:1, and 40:1 were represented in every GG class. Ceramide 32:1 seemed to be specific of GD3, while ceramides 34:2, 41:1, and 42:2 were found only in GM3 and GD3.

#### Assessment of the molecular species distribution in the major GG classes

The use of SRM in the negative mode with QqQ mass spectrometer enabled us to quantify the distribution of the different GG molecular species. The proportion of each molecular species was expressed as the ratio of its peak area

on the ion chromatogram to the sum of all detected peak areas in its GG class, every GG class being considered separately. The method was first validated using both a mixture of commercial GG standards and a sample of rat retina GGs in order to account for matrix effect. Between-day and within-day precision results are given in supplementary Tables 1 and 2. For mixture of GG standards, most of the coefficient of variation (CV) values were below 5%. For rat retina GG, CV values were higher, but most of them were below 20%. The highest CV values were observed for low-proportion molecular species and in GG classes that exhibited the lowest signal intensities in LC/MS (GD1a, GD1b, and GQ1b). Overall, our method offers a reliable way to determine the relative distribution of the molecular species present in the various GG classes. However, if the method is to be used to compare the relative distribution of GG species between different biological samples, we consider it will not be reliable for species presenting a CV value higher than 20%. The relative distribution of GG species of rat retina given in Fig. 4 reveals discrepancies among the different GG classes. However, ceramide 36:1 and 38:1 consistently appeared to be the two major ones, except for GM3 and GD3. In the tetraosylgangliosides (GD1a, GD1b, GT1b, and GQ1b), ceramide 36:1 and ceramide 38:1 accounted respectively for 66% to 71% and 11% to 27% of all molecular species detected. The presence of ceramide 34:1 in large amount (34% of all species detected) seemed to be a specificity of GD3, which also contained a high proportion of ceramide 36:1 (43% of all species detected) and ceramide 38:1 (12% of all species detected). GM3 exhibited a more diverse distribution with similar proportions of ceramides 34:1 (17% of all species detected), 36:1 (19%), 38:1 (18%), 40:1 (12%), and 42:1 (15%). Even if the percentage values varied to some extent, those results are overall in accordance with a recently published study analyzing the lipiome of rat retina by a different MS method (direct infusion, nanospray, positive/negative ionization full scan) (31). They observed the same three major species in GD3 and ceramide 36:1 and 38:1 as the major ones in GD1 and GT1b classes. However, they detected only ceramides 34:1 and 36:1 in GM3 and did not detect ceramide 38:1 in

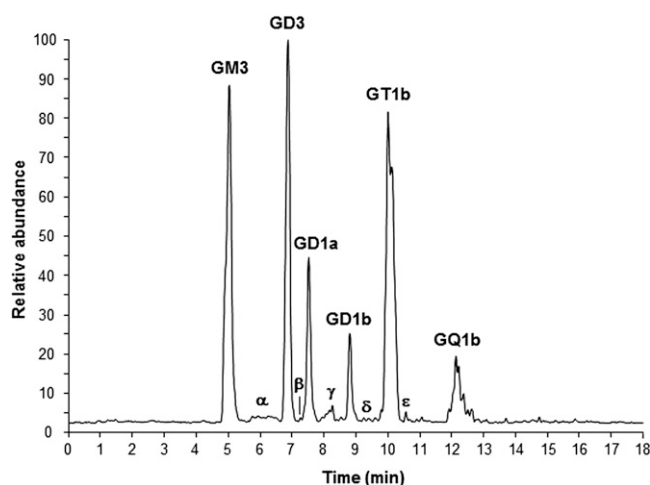


**Fig. 3.** QqQ HILIC/ESI/MS/MS chromatogram of a GG extract of rat retina. The mass spectrometer was operated in the negative precursor ion mode of the ion  $m/z$  290 corresponding to NANA.  $\alpha$ ,  $\beta$ ,  $\gamma$ ,  $\delta$ , and  $\epsilon$  refer to unidentified NANA-containing compounds.

TABLE 3. Molecular species of the major GG classes detected in precursor ion scanning with the QqQ mass spectrometer

Ceramide	<i>m/z</i>	<i>M</i>	<i>E<sub>c</sub></i> (V)
GM3 [M-H] <sup>-</sup>			
34:2	1,149.7	1,150.698	48
34:1	1,151.7	1,152.713	48
36:2	1,177.7	1,178.729	48
36:1	1,179.7	1,180.744	48
38:2	1,205.7	1,206.760	48
38:1	1,207.7	1,208.776	48
40:2	1,233.8	1,234.791	48
40:1	1,235.8	1,236.807	48
41:1	1,249.8	1,250.823	48
42:2	1,261.8	1,262.823	48
42:1	1,263.8	1,264.838	48
GD3 [M-2H] <sup>2-</sup>			
32:1	706.9	1,415.777	30
34:2	719.9	1,441.793	30
34:1	720.9	1,443.809	30
36:2	733.9	1,469.824	30
36:1	734.9	1,471.840	30
38:2	747.9	1,497.856	30
38:1	748.9	1,499.871	30
40:2	761.9	1,525.887	30
40:1	763.0	1,527.902	30
41:1	769.9	1,541.918	30
42:2	776.0	1,553.918	30
42:1	777.0	1,555.934	30
GD1a [M-2H] <sup>2-</sup>			
34:1		1,808.941	40
36:2		1,834.956	40
36:1	917.5	1,836.972	40
38:2	930.5	1,862.988	40
38:1	931.5	1,865.003	40
40:2	944.5	1,891.019	40
40:1	945.5	1,893.035	40
GD1b [M-2H] <sup>2-</sup>			
34:1	903.5	1,808.941	40
36:2	916.5	1,834.956	40
36:1	917.5	1,836.972	40
38:2	930.5	1,862.988	40
38:1	931.5	1,865.003	40
40:2	944.5	1,891.019	40
40:1	945.5	1,893.035	40
GT1b [M-2H] <sup>2-</sup>			
34:1	1,049.0	2,100.036	30
36:2	1,062.0	2,126.052	30
36:1	1,063.0	2,128.067	30
38:2	1,076.0	2,154.083	30
38:1	1,077.0	2,156.099	30
40:1	1,091.1	2,194.130	30
42:1	1,105.1	2,211.154	30
GQ1b [M-3H] <sup>3</sup>			
34:1	796.0	2,393.147	30
36:2	804.7	2,417.147	30
36:1	805.4	2,419.163	30
38:2	814.1	2,445.179	30
38:1	814.7	2,447.194	30
38:1	814.7	2,447.194	30
40:1	824.1	2,475.226	30

*M*, molecular ion isotopic mass.

GQ1b. For every GG classes, it seems we were able to detect more different molecular species, especially the ones expressed in low proportions.

#### Ceramide characterization of the major GG classes by HRMS

Theoretically, a GG molecular species (e.g., 36:1) can exist in different combinations of LCB and FA (e.g., d16:1/20:0, d18:1/18:0, d18:0/18:1, d20:1/16:0). HRMS with LTQ-Orbitrap enabled us to distinguish between different

GG molecular species with the same molecular mass (isobaric ceramides) thanks to fragmentation of GG molecules (MS/MS) and further detection of the LCB present in each ceramide moiety. Associated FA could then be deduced based on the exact mass of the molecule. The fragmentation spectrum of GD3 is given as an example in **Fig. 5**. Results, summarized in **Table 4**, revealed that three distinct LCBs coexisted in rat retina GGs: d18:1, d20:1, and d18:2. Sphingosine (d18:1) was by far the most widely represented. It was found in every GG class, unlike d20:1 LCB, which was more specifically detected in GD1a and GD1b, although in minor proportion in GD3 and GT1b as well. The d18:2 was found exclusively in GM3. In contrast with standards of GM3 and GD3 originated from bovine buttermilk (data not shown), d16:1 was absent in rat retina GGs. Of note, traces of d17:0 could also be detected in GM3 and GD3. As for the FAs, they were more diverse (8 different types), saturated or monounsaturated, ranging from 16 to 24 carbons. However, 18:0 was the most abundant FA found in rat retina GGs. GM3 and GD3 molecular species also contained 16:0 and 20:0 in significant proportions. The 20:0 FA was found in GT1b as well. Those results are overall in accordance with older data obtained in bovine retina using gas chromatography (32), which described d18:1 as the major LCB in GD3, while GD1a, GD1b, and GT1b LCB were distributed between d18:1 and d20:1. However, some discrepancies appear in the FA distribution. The 18:0 remained the major FA, followed by 20:0, but the authors reported higher proportions of 22- and 24-carbon FAs. Also, they did not detect any 16:0 FA. These differences might be due to animal species particularities. Moreover, while our LC/MS technique ensured that the molecules analyzed are GG, gas chromatography results could be polluted by contaminants still present in the sample, such as phospholipids, after the GG extraction procedure. In the gas chromatography analyses, LCBs and FAs were analyzed and identified separately. Thus, the technique did not allow determining the ceramide type. On the contrary, the LC/MS method we developed allowed determining which LCB was associated with which FA. Overall, d18:1/18:0 appeared to be the most frequently found ceramide type in rat retina GG: almost 20% of GM3 molecular species, >43% of GD3 molecular species, and ~70% of GD1a, GD1b, and GT1b ceramide types. The d18:1/16:0 was the second most important ceramide species in GD3 (34%) and GM3 (20%), while it was very minor in GD1a, GD1b, and GT1b. In place of d18:1/16:0, d20:1/18:0 was the second most abundant type in GD1a and GD1b, while it was absent or very minor in GM3, GD3, and GT1b. The d18:1/20:0 was the second most abundant ceramide in GT1b (26%), while it accounted for only 12% of GD3 ceramide types and was minor in GD1a and GD1b. It was also important in GM3 (18%). GQ1b molecular species could not be characterized due to their low amount.

#### Identification of the minor classes of GGs

The high variability in the oligosaccharidic chain results in a huge number of distinct GGs. A full scan in positive

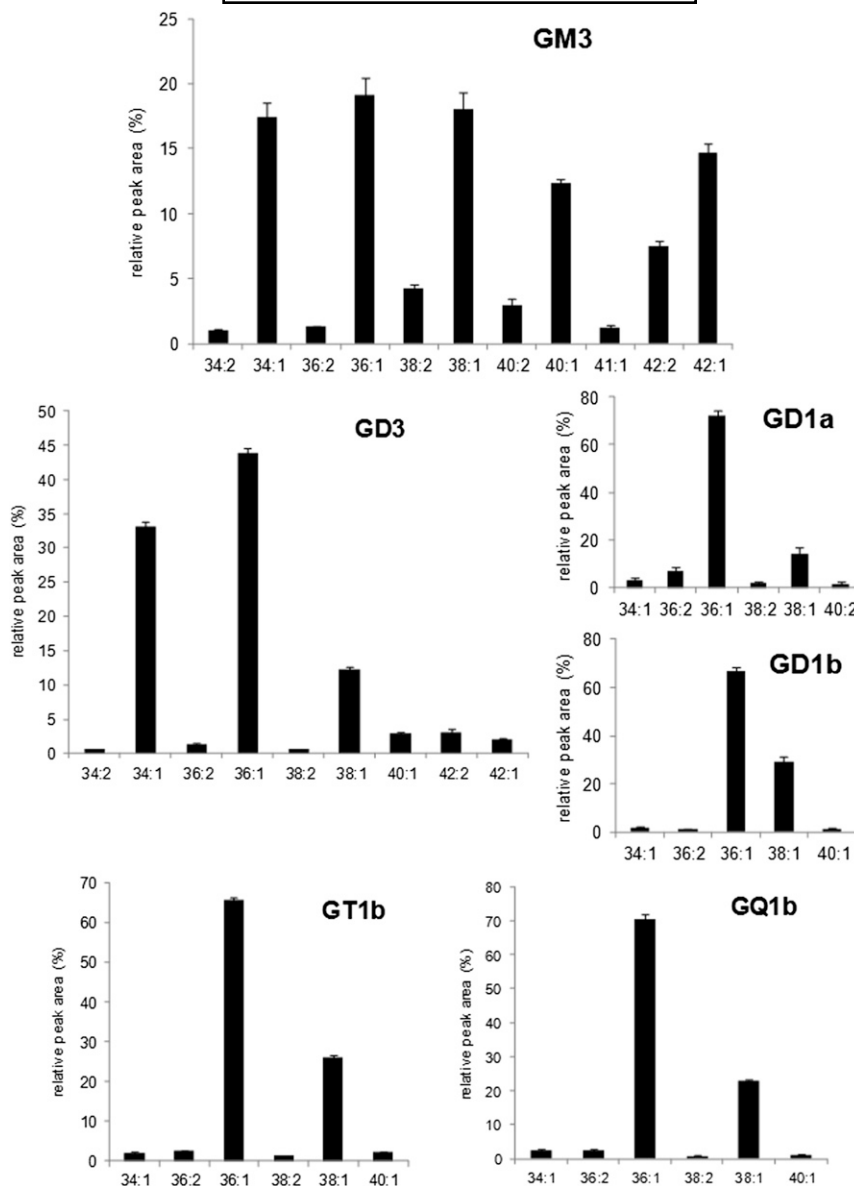


**Fig. 4.** Molecular species distribution of the major GG classes of rat retina. The percentage of each ceramide species is expressed relatively to the sum of all detected species in its specific GG class, every GG class being considered separately. Data were obtained by operating the QqQ mass spectrometer in negative SRM. Among molecular species detected in precursor ion scanning (Table 3), only species with signal/noise >10 were considered in SRM. Results are expressed as mean  $\pm$  SD of four independent samples injected three times in LC/MS.

mode using the high-resolution mass spectrometer LTQ-Orbitrap enabled us to detect and identify less abundant and less frequently reported GGs, for which no commercial standard is available. This is illustrated in **Fig. 6** showing ion chromatograms of 36:1 ceramide types of every di-, tri-, and quadrisialylated GG detected. The 36:1 ceramide was chosen because it was the major one in our rat retina GG extracts. On top of GD3, GD1a, GD1b, GT1b, and GQ1b, analyses revealed an additional GG class, GT3. Its retention time in between GD1a and GD1b led us to think that it corresponded to the unidentified band previously detected in HPTLC (Fig. 2) and in LC/MS with the QqQ mass spectrometer (Fig. 3, peak  $\gamma$ ). Moreover, it revealed the presence of acetylated forms of some GG classes, especially

acetylated GD3, GT3, GT1b, and GQ1b. Analysis of the MS<sup>2</sup> fragmentation spectra of the major 36:1 molecular species of acetylated GD3 and GT3 revealed that the acetylation was carried by the last sialic acid for GD3 and alternatively by the last and the middle sialic acid for GT3. This observation suggested that acetylated GT3 could result from both acetylation of GT3 and sialylation of acetylated GD3. Those newly identified GG classes corresponded to the unknown peaks observed in LC/MS with the QqQ mass spectrometer  $\alpha$ ,  $\beta$ ,  $\delta$ , and  $\epsilon$ , respectively (Fig. 3). Very minor amounts of acetylated GD1a and GD1b could also be detected. However, we did not detect any acetylated forms of monosialylated GG. Of note, we did not detect N-glycolylneuraminic acid containing GG in our samples,

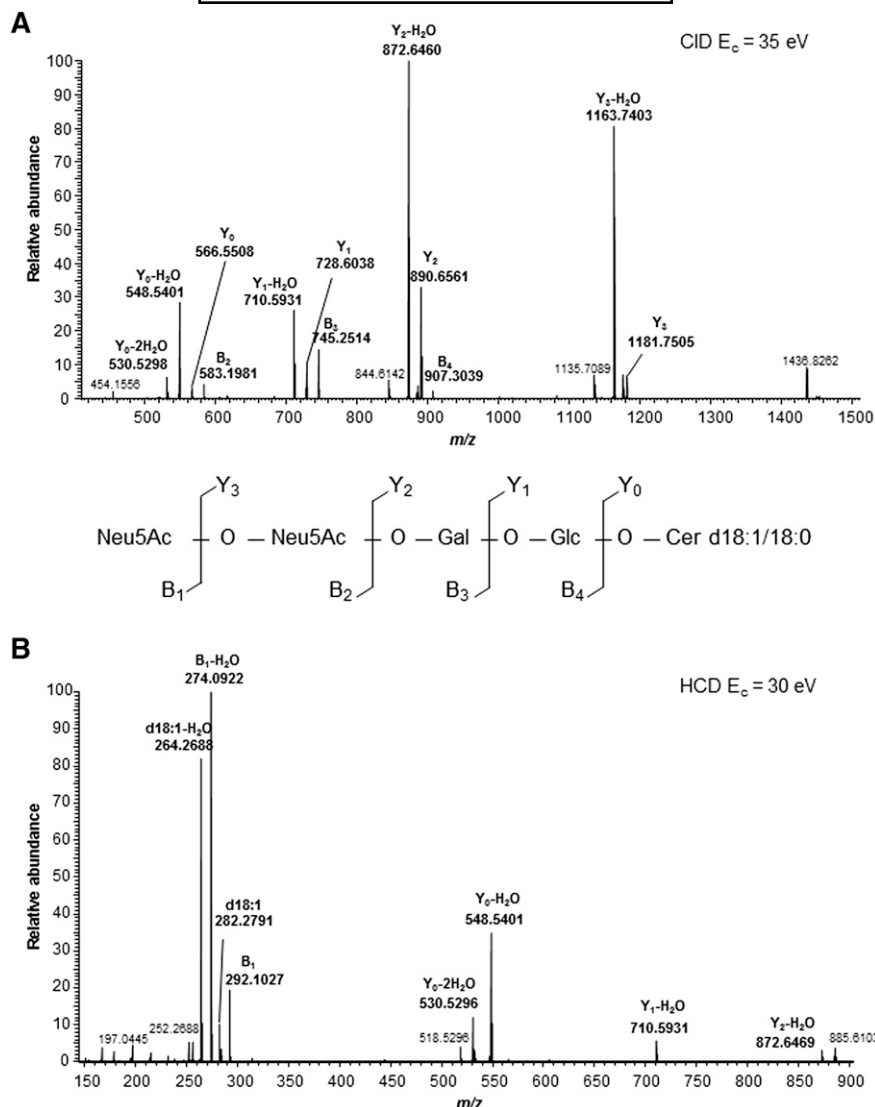


**Fig. 5.** LTQ-Orbitrap fragmentation spectrum of GD3 36:1 GG of rat retina. The mass spectrometer was operated in positive full scan mode. Structural analysis of the  $[M+H]^+$  ion corresponding to GD3 36:1 at  $m/z$  1,472.847 by multistage. A: CID  $MS^2$  at  $E_c = 35$  eV. B: HCD  $MS^2$  at  $E_c = 30$  eV.

and NANA was the only form of sialic acid present in rat retina GGs. HRMS also enabled the identification of the ceramide types present in these GG classes. A list of every molecular species detected is given in **Table 5**. As for the major classes, ceramides ranged from 34 to 42 carbons, with one or two unsaturations. Overall, acetylated forms of GGs existed in a lower diversity of ceramide types (2 to 7) than the nonacetylated ones. Ceramides 36:1 and 38:1 were found in every major and minor GG classes.

#### Assessment of the molecular species distribution in the minor GG classes

As for the major GG classes, the QqQ mass spectrometer was used in SRM mode to quantify the distribution of the different GG molecular species of the minor GG classes. The precursor and product ion pairs were selected based on the LTQ-Orbitrap results, but some species were not considered in SRM because they stand below the quantification limit (signal/noise <10; see Table 5). Results are

given in **Fig. 7**. Except for the GT3 class in which the acetylated form accounted for >30% of all molecular species, acetylated GG remained very minor in our analytical conditions (6% for GQ1b, 1.6% for GT1b, and 0.4% for GD3). For acetylated GD3, GT1b, and GQ1b, the major ceramide types were the same as those found in the corresponding nonacetylated classes: ceramides 34:1 (12% of all ceramide molecular species detected), 36:1 (75%), and 38:1 (13%) for acetylated GD3; ceramides 36:1 and 38:1 for acetylated GT1b and GQ1b. Those observations corroborated the results of Lydic et al. (31) except that these authors did not detect ceramide 38:1 in acetylated GQ1b. They also reported a much higher proportion of acetylated GG, especially for GT1b and GQ1b. The distribution we observed for the acetylated GT3 appeared to be more surprising. Indeed, ceramide 36:2 was the major type found in acetylated GT3 (36% of all ceramide molecular species detected), while it was very minor in GT3 (1%). Moreover, ceramide 42:1, which was among the most abundant in

TABLE 4. Ceramide species of the major GG classes characterized by HRMS with the LTQ-Orbitrap

Ceramide	GM3	GD3	GD1a	GD1b	GT1b
34:2	<b>d18:1/16:1</b>	<b>d18:1/16:1</b>	NR	NR	NR
34:1	<b>d18:1/16:0</b>	<b>d18:1/16:0</b>	<b>d18:1/16:0</b>	<b>d18:1/16:0</b>	<b>d18:1/16:0</b>
36:2	<b>d18:1/18:1</b>	<b>d18:1/18:1</b>	<b>d18:1/18:1</b>	<b>d18:1/18:1</b>	<b>d18:1/18:1</b>
36:1	<b>d18:1/18:0</b>	<b>d18:1/18:0</b>	<b>d18:1/18:0</b>	<b>d18:1/18:0</b>	<b>d18:1/18:0</b>
38:2	d18:1/20:1	<b>d18:1/20:1</b>	<b>d18:1/20:1</b>	NR	d18:1/20:1
	d18:2/20:0				d20:1/18:1
38:1	<b>d18:1/20:0</b>	<b>d18:1/20:0</b>	<b>d20:1/18:0</b>	<b>d20:1/18:0</b>	<b>d18:1/20:0</b>
		d20:1/18:0	d18:1/20:0	d18:1/20:0	
40:2	<b>d18:1/22:1</b>	NR	<b>d18:1/22:1</b>	<b>d20:1/20:1</b>	NR
	d18:2/22:0		d20:1/20:1	d18:1/22:1	
40:1	<b>d18:1/22:0</b>	<b>d18:1/22:0</b>	<b>d20:1/20:0</b>	<b>d20:1/20:0</b>	NI
			d18:1/22:0		
42:2	d18:1/24:1	<b>d18:1/24:1</b>	NR	NR	NR
	d18:2/24:0				
42:1	<b>d18:1/24:0</b>	<b>d18:1/24:0</b>	NR	NR	NR

NI, nonidentified; NR, nonrepresented. Major molecular species are indicated in bold.

GT3 (21%), was undetectable in acetylated GT3. Of note, the low amount of some minor GG classes (acetylated GD1a and GD1b) did not permit a reliable quantification of the distribution of the ceramide types.

## DISCUSSION

GG analysis faces many difficulties. First, GGs exhibit an original and complex biochemical structure, containing both a hydrophilic and a hydrophobic moiety. They are glycosphingolipids and belong to both the glycome and the lipidome. Second, GGs make up a very wide and diverse family of molecules due to the heterogeneity of both the oligosaccharidic chain and the ceramide moiety. Third, they are expressed in low abundance in plasma membranes, especially relatively to the other amphiphatic components of membranes that are phospholipids.

Densitometric analysis of HPTLC plates after resorcinol revelation has long been considered a gold standard for the study of GG and is still widely used. It gives an image of the GG pattern of a biological sample. Yet, the approach chosen to analyze the HPTLC plates and express the results will affect the conclusions drawn regarding the GG distribution. GD3 is thus usually considered the most abundant GG in mammalian retina (26–28, 33). This is based on direct evaluation of signal intensities by scanning resorcinol-stained HPTLC plates. The proportion of each GG class is determined by the ratio of its peak area to the sum of every peak, corresponding to the total GG-bound sialic acid detected on the plate. However, as for the GG-NANA content assay, which aims at measuring in solution the total amount of sialic acid, the detection is based on the colorimetric reaction between resorcinol and sialic acid. While this reaction should not be impacted by the ceramide types of the GG, it is to some extent dependent

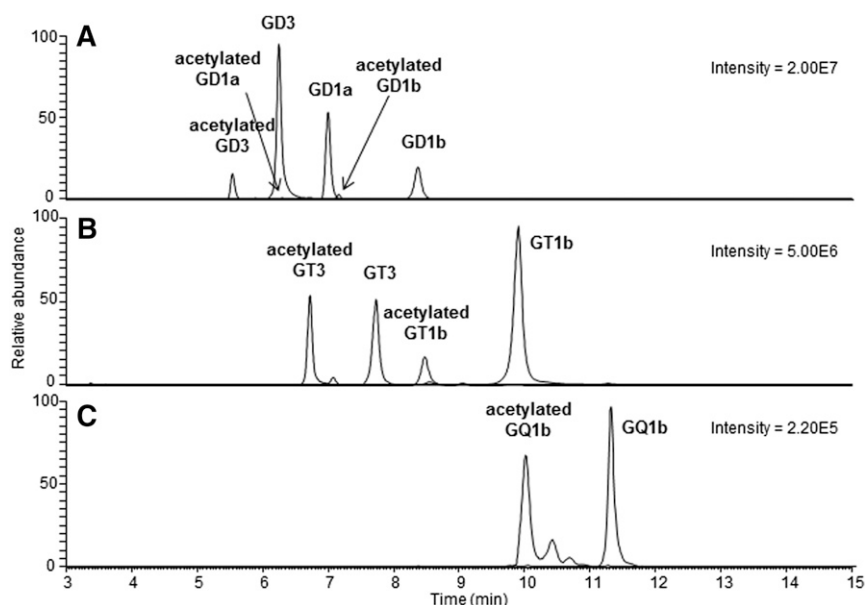


Fig. 6. LTQ-Orbitrap HILIC/ESI/MS chromatograms of rat retina GGs. The mass spectrometer was operated in positive full scan mode. The extracted ion chromatograms of 36:1 species of disialylated GGs (A), trisialylated GGs (B), and quadrisialylated GGs (C) are shown.

TABLE 5. Molecular species of the minor GG classes detected with the HRMS LTQ-Orbitrap and selected for SRM analyses using the QqQ mass spectrometer

Ceramide	Orbitrap			QqQ		
	[M+H] <sup>+</sup> <sub>exp</sub>	[M+H] <sup>+</sup> <sub>theo</sub>	Mass Error (ppm)	m/z	M	E <sub>c</sub> (V)
Acetylated GD3				[M-2H] <sup>2-</sup>		
34:1	1,486.8249	1,486.8264	1.0	741.9	1,485.819	30
36:2	1,512.8408	1,512.8420	0.8	754.9	1,513.850	30
36:1	1,514.8562	1,514.8577	1.0	755.9	1,513.850	30
38:1	1,542.8863	1,542.8890	1.7	769.9	1,541.882	30
40:1	1,570.9199	1,570.9203	0.2	783.9	1,569.913	30
Acetylated GD1a				[M-2H] <sup>2-</sup>		
36:1	1,879.9868	1,879.9902	1.8	938.5	1,878.983	30
38:1	1,908.0176	1,908.0215	2.1	952.5	1,907.014	30
Acetylated GD1b				[M-2H] <sup>2-</sup>		
36:1	1,879.9871	1,879.9902	1.7	938.5	1,878.983	30
38:1	1,908.0159	1,908.0215	3.0	952.5	1,907.014	30
GT3				[M-2H] <sup>2-</sup>		
34:2	1,733.8960	1,733.8956	-0.2	865.5	1,732.888	30
34:1	1,735.9102	1,735.9113	0.6	866.5	1,734.904	30
36:2	1,761.9244	1,761.9269	1.4	879.5	1,760.920	30
36:1	1,763.9404	1,763.9426	1.2	880.5	1,762.935	30
38:2	1,789.9512	1,789.9582	3.9	893.5	1,788.951	30
38:1	1,791.9703	1,791.9739	2.0	894.5	1,790.967	30
40:1	1,819.9985	1,820.0052	3.7	920.5	1,818.998	30
42:2	1,846.0168	1,846.0208	2.2	921.5	1,845.014	30
42:1	1,848.0349	1,848.0365	0.9	922.5	1,847.029	30
Acetylated GT3				[M-2H] <sup>2-</sup>		
34:1	1,777.9207	1,777.9218	0.6	887.5	1,176.915	30
36:2	1,803.9327	1,803.9375	2.7	900.5	1,802.930	30
36:1	1,805.9120	1,805.9531	1.1	901.5	1,804.946	30
38:2	1,831.9555	1,831.9688	7.3	914.5	1,830.962	30
38:1	1,833.9827	1,833.9844	0.9	915.5	1,832.977	30
40:1	1,862.0143	1,862.0157	0.8	929.5	1,861.008	30
42:2	1,888.0271	1,888.0314	2.3	942.5	1,887.024	30
Acetylated GT1b				[M-2H] <sup>2-</sup>		
34:1	2,143.0591	2,143.0539	-2.4	1,070.0	2,142.047	40
36:2	2,169.0758	2,169.0696	-2.9	1,083.0	2,006.010	40
36:1	2,171.0877	2,171.0852	-1.2	1,084.0	2,170.078	40
38:1	2,199.1164	2,199.1165	0.0	1,098.0	2,198.109	40
40:1	2,227.1449	2,227.1478	1.3	1,112.0	2,226.141	40
Acetylated GQ1b				[M-3H] <sup>3-</sup>		
36:1	2,462.1812	2,462.1812	0.0	819.4	2,461.174	30
38:1	2,490.2110	2,490.2125	0.6	828.7	2,489.205	30

exp, experimental; theo, theoretical.

on the GG class, and it tends to underestimate the representation of the most complex GGs, as we report here. For this reason, it is more accurate to quantify each GG according to the reaction of its own class, by establishing calibration curves. In this way, we showed that, in rat retina, GD3 is actually represented in equal proportion to GD1b and GT1b, the two other b-series GGs. It remains that GD3 abundance seems to be a specificity of the mammalian retina. Indeed, chick retina, as other types of nervous tissues, especially brain, contain mainly tetraosylgangliosides (GM1, GD1a, GD1b, and GT1b) (9, 27, 33, 34). Another limitation of this analytical technique stands in the uncertainty of GG identification, based on comigration with standards and to the resolution of the chromatography, which might not be sufficient to separate some GG classes that would coelute. Moreover, the sensitivity of HPTLC coupled to colorimetric detection is quite low (~25 pmol sialic acid), and the method is not convenient for the analysis of large numbers of samples. Finally, it does not provide information on the structure of the molecule (acetylation and ceramide type).

The emergence of LC/MS techniques in the field of glycosphingolipids analysis enabled us to overcome some of these limitations. Especially, it provided a much higher level of precision and sensitivity into the analysis of GGs. Techniques are based on the separation of GGs by LC followed by detection and measurement of the molecular species using a mass spectrometer.

Chromatographic separation prior to MS analysis enables us to distinguish between isomeric and isobaric species (i.e., GD1a and GD1b), which could not be distinguished by MS alone. Additionally, a suitable chromatographic separation decreases the number of compounds to be analyzed at the same time in the mass spectrometer and may thus reduce any ionization suppression, increasing the sensitivity of the detection. The impact of the presence of contaminants in the sample, especially phospholipids, on GG ionization in the mass spectrometer is rather controversial. Lydic et al. (31), for example, claim that the ion suppression is modest and that shotgun ESI/MS on total lipid extracts is an effective method for the analysis of rat retina lipidome, including GGs. This

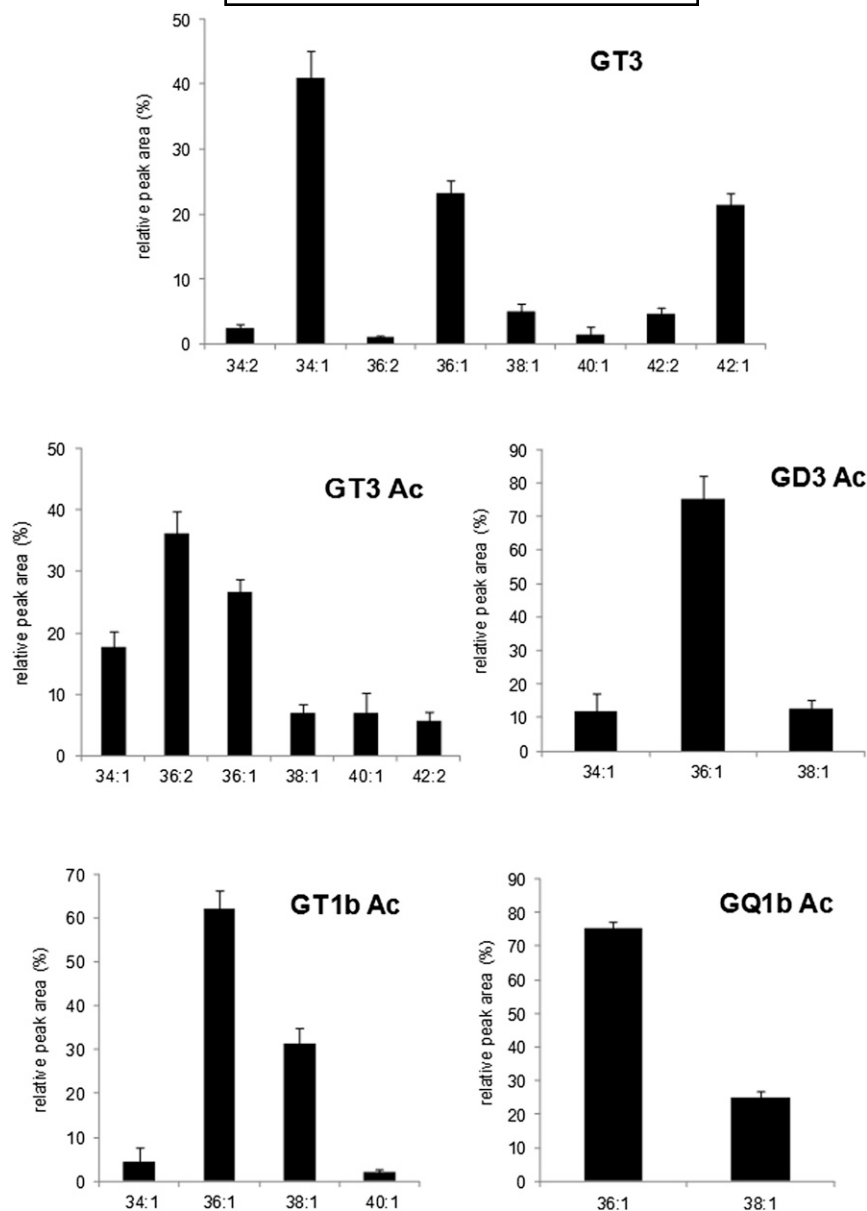


**Fig. 7.** Molecular species distribution of the minor GG classes of rat retina. The percentage of each ceramide species is expressed relatively to the sum of all detected species in a specific GG class, every GG class being considered separately. Data were obtained by operating the QqQ mass spectrometer in negative SRM. Among molecular species detected in Orbitrap (Table 5), only species with signal/noise >10 were considered in SRM. Results are expressed as mean  $\pm$  SD of four independent samples injected three times in LC/MS.

was based on the similarities observed between the lipid profile of total lipid extracts and GG-enriched extracts. On the contrary, other authors reported a suppression of GG precursor ion signal to  $\sim 14\%$  of the original intensity by addition of dioleoylphosphatidylcholine in the analyte (35). This result was corroborated by Huang et al. (36) who also showed important suppression of the GG signals (from 22% to 51% extinction for GM2, GM3, GD2, and GD3) due to contaminants present in the extracts prepared by simple protein precipitation procedure by comparing MS signals of spiked GG standards in analyte-free extracts and in pure solvents. To avoid any potential suppression, we preferred a sample extraction aiming at depleting phospholipids and enriching the extract with GGs.

We performed a biphasic extraction procedure adapted from Svennerholm et al. (37). Sample preparation makes a critical point when studying GGs. Specific losses of classes or species can occur because the molecular heterogeneity of GGs results in heterogeneity in their physicochemical properties. This issue, per se, was not under the scope of this study, which focused on the analytical part. Regarding the chromatography, we implemented an HPLC method in HILIC conditions using a silica column to efficiently separate GGs based on their oligosaccharidic chain (i.e., according to their class). This had already been reported, most recently by Ikeda et al. (30), with an NH<sub>2</sub> column and ACN/ammonium formate as mobile phase (29). We noticed that our method resulted in very repeatable

retention times. This method appeared to be convenient for the identification of every molecular species in a GG class because they eluted grouped within a short interval of time, contrary to HPLC methods based on reversed-phase, which separate GGs mainly according to their carbon number resulting in multiple peaks for each specific GG class (38).


MS/MS was used after ESI. This soft ionization technique induces little fragmentation in the ion source and leads to a signal proportional to the quantity of analytes. Thus, it is an appropriate method for quantitation. MS/MS results in the production of an abundant predominant fragment ion characteristic of GG, NANA (sialic acid) at  $m/z$  290 (23, 35). We used a QqQ mass spectrometer as well as a high-resolution LTQ-Orbitrap mass spectrometer as mass analyzers. These apparatuses offered a GG identification that was much more reliable than HPTLC associated to colorimetric revelation because it is based on the detection of a specific fragment ion common to every GG class and on the exact mass of the molecule. It gave us confirmation regarding the identity of the GG classes of rat retina we previously observed in HPTLC (GM3, GD3, GD1a, GD1b, GT1b, and GQ1b). In addition, high resolution enabled us to identify unknown classes for which no commercial standard is available. We thus identified GT3 and acetylated forms of many GG classes: GD3, GT3, GD1a, GD1b, GT1b, and GQ1b. In terms of sensitivity, LC/MS is about a hundred times more efficient than HPTLC coupled to resorcinol revelation because it enables GG detection in the range of tenths of picomoles of sialic acid. Moreover, the advent of MS nowadays offers great possibilities to perform glycolipidomic studies and apprehend more easily the huge diversity of GGs. In particular, it enables us to scan the variety of GG molecular species by characterizing their ceramide moiety. The first reports using MS go back to the 1990s with structural characterization of a single GG (39, 40). Profiling studies really started quite recently (30, 38). Previous data on ceramide composition of retinal GGs were obtained in the late 1970s with indirect and less efficient techniques. Authors identified FAs, on one hand, and LCBs, on the other hand, using gas chromatography techniques (32). Thanks to the MS techniques described here, including high resolution, we were able to identify combinations of FAs and LCBs and determine the distribution of the different ceramide types among a GG class. This fine analysis will help decipher the role of the variability of the ceramide moiety in GGs, which is gaining interest with the emergence of the raft concept in cellular signaling. The current view is that plasma membrane contains organized microdomains enriched in cholesterol, sphingolipids, including GGs, and signaling proteins forming platforms implicated in membrane signaling and trafficking (41). Specific microdomains called glycosynapses have been described as specially enriched in GGs (8, 42), and GG biological functions are more and more considered to be linked to their presence in these microdomains and to their capacity to modulate the functioning of these signaling platforms (42, 43). GGs are anchored into membrane microdomains through

their ceramide moiety, so it is likely that the ceramide type will influence GG presence within specific microdomains and their interaction with signaling partners. It will thus be of interest to understand how differences in ceramide types will affect GG biological functions. Besides, MS data will offer new perspectives to better understand the metabolism of GGs. Especially, the characterization of ceramide types and their distribution will reveal how the proportion of GG ceramide molecular species fluctuate during the course of GG biosynthesis and thus provide information regarding biosynthetic pathways of GGs and their modified forms. It will also give clues to help us understand the biosynthetic connections between the different GG classes. We revealed that ceramide 38:1, for example, did not actually correspond to the same major molecule in GM3, GD3, and GT1b on one hand (d18:1/20:0), and in GD1a and GD1b on the other hand (d20:1/18:0). It thus seems that precursor GGs with a specific type of ceramide are preferentially used to give rise to specific GG products along the biosynthetic scheme. However, the discrepancies observed between the ceramide profile of GD3 and GD1b and the similarities between GD1a and GD1b are quite intriguing. Indeed, GD1b belongs to the same b-series GGs as GD3, which is its precursor. On the other hand, GD1a and GD1b are isomers but belong to different GG series and thus do not share the same precursor. The discrepancies we highlighted between the molecular species distribution of GT3 and its acetylated form were also unexpected. Besides, it appears that this molecular species distribution is specific to the tissue because the pattern we describe here for rat retina is completely different from the one reported by Ikeda et al. (38) in mouse brain. Of note, they also observed differences in the ceramide profile of GD3 and its precursor GM3 using similar techniques. No doubt, current knowledge regarding GG biosynthetic pathways will be enriched by the new pieces of information that will result from the development of powerful analytical techniques such as LC/MS.

While MS offers new perspectives into GG analysis, pure standards to be used as internal standards as well as individual standards to establish calibration curves are still missing from commercial sources. They are required to normalize for differences in extraction efficiency as well as differences in ionization and fragmentation of GG classes and individual molecular species in order to achieve a proper absolute quantification. Indeed, regarding the detection, we observed that the signal response of the different GG classes with the QqQ mass spectrometer varies quite importantly. The intensity of a GG class peak is not directly proportional to its absolute amount in the sample, relatively to the other GG classes but reflects the response of this specific GG class in MS. This is illustrated in supplementary Fig. 3. Monosialogangliosides give a high signal, whereas polysialogangliosides such as GD1b and GQ1b tend to give a low signal. These discrepancies could be due to differences in ionization, fragmentation, and formation of mono- or multicharged ions under our conditions. It is thus not appropriate to rely on this technique to compare

the amount of a GG class with other classes present in a sample, without using adequate standards. The monosialo deuterated GGs are the only commercially available compounds to be used as internal standards to date (GM3d3, GM2d3, and GM1d3), and they unfortunately cannot be used as proper standards for other GG classes than GM3, GM2, and GM1, respectively. Most of the studies published in the literature do not actually use any internal standard (44–46). Some have used GM3d3 for various GG classes (GM3, GM2, GD3, and GD2) in human plasma (36) or GM1d3 for GM2 in cells and plasma (47), while others have used phospholipids (30, 31). Recently, authors reported the synthesis of GG-bearing nonnatural FAs for the major classes of mammalian brain and also some tumor-associated classes, which will be valuable tools to use as internal standards for MS analyses (48). For quantification purposes, authors used commercial standards they considered to be representative of the GG molecular species present in their samples to spike their extracts. Giuffrida et al. (46) used bovine milk GM3 and GD3 for quantification of GM3 and GD3 in human milk, respectively. Huang et al. (36) used bovine milk GM3 and GD3 and human brain GM2 and GD2 for the same GG classes in human plasma. Fuller et al. (47) used human GM2 standard for GM2 in human fibroblasts, leukocytes, and plasma. However, most of them agreed that absolute quantification of the different GG molecular species would have required standards identical in structure (ceramide type) to the molecules to quantify to account for the variation in extraction during the sample preparation as well as in MS signal response.

## CONCLUSION

GGs, the most complex of the sphingolipids, so called as a reference to the legendary Sphinx because of their dual and mysterious nature, are far from having unveiled all their secrets. This is linked to the difficulties that GG analysis faces due to the complexity and heterogeneity of these molecules. We make here our contribution by reporting a comprehensive approach to analyze the wide diversity of GGs in biological samples. Especially, we describe a targeted analytical method that allows for the determination of the individual molecular species distribution in each GG class. Moreover, using HRMS, we describe further characterization of the ceramide moiety of GG molecules as well as identification of minor GG classes. Those methods provide the basis for a better understanding of the biological roles of GGs, especially the roles of the ceramide variability, which remains so far quite unclear. 

The authors thank the animal facility of Centre des Sciences du Goût et de l'Alimentation for animal care, Niyazi Acar for technical help during rat retina dissection, Stephanie Cabaret (Centre des Sciences du Goût et de l'Alimentation) and Marie-José Penouilh (Institut de Chimie Moléculaire) for technical assistance, and Alain Tabard (Institut de Chimie Moléculaire) for granting access to the LTQ-Orbitrap mass spectrometer.

- Klenk, E. 1942. Über die Ganglioside, eine neue Gruppe von zuckerhaltigen Gehirnlipoiden. *Z. Physiol. Chem.* **273**: 76–86.
- Yu, R. K., M. Yanagisawa, and T. Ariga. 2007. Glycosphingolipid structures. In *Comprehensive Glycoscience*. J. P. Kamerling, editor. Elsevier, Amsterdam. 73–120.
- Degroote, S., J. Wolthoorn, and G. van Meer. 2004. The cell biology of glycosphingolipids. *Semin. Cell Dev. Biol.* **15**: 375–387.
- Simons, K., and M. J. Gerl. 2010. Revitalizing membrane rafts: new tools and insights. *Nat. Rev. Mol. Cell Biol.* **11**: 688–699.
- Simons, K., and E. Ikonen. 1997. Functional rafts in cell membranes. *Nature*. **387**: 569–572.
- Simons, K., and D. Toomre. 2000. Lipid rafts and signal transduction. *Nat. Rev. Mol. Cell Biol.* **1**: 31–39.
- Sonnino, S., L. Mauri, V. Chigorno, and A. Prinetti. 2007. Gangliosides as components of lipid membrane domains. *Glycobiology*. **17**: 1R–13R.
- Hakomori, S., and Y. Igarashi. 1995. Functional role of glycosphingolipids in cell recognition and signaling. *J. Biochem.* **118**: 1091–1103.
- Yu, R. K., Y. T. Tsai, and T. Ariga. 2012. Functional roles of gangliosides in neurodevelopment: an overview of recent advances. *Neurochem. Res.* **37**: 1230–1244.
- Ohmi, Y., O. Tajima, Y. Ohkawa, Y. Yamauchi, Y. Sugiura, and K. Furukawa. 2011. Gangliosides are essential in the protection of inflammation and neurodegeneration via maintenance of lipid rafts: elucidation by a series of ganglioside-deficient mutant mice. *J. Neurochem.* **116**: 926–935.
- Sheikh, K. A., J. Sun, Y. Liu, H. Kawai, T. O. Crawford, R. L. Proia, J. W. Griffin, and R. L. Schnaar. 1999. Mice lacking complex gangliosides develop Wallerian degeneration and myelination defects. *Proc. Natl. Acad. Sci. USA*. **96**: 7532–7537.
- Tajima, O., N. Egashira, Y. Ohmi, Y. Fukue, K. Mishima, K. Iwasaki, M. Fujiwara, J. Inokuchi, Y. Sugiura, and K. Furukawa. 2009. Reduced motor and sensory functions and emotional response in GM3-only mice: emergence from early stage of life and exacerbation with aging. *Behav. Brain Res.* **198**: 74–82.
- Kolter, T., and K. Sandhoff. 2006. Sphingolipid metabolism diseases. *Biochim. Biophys. Acta*. **1758**: 2057–2079.
- Simpson, M. A., H. Cross, C. Proukakis, D. A. Priestman, D. C. Neville, G. Reinkensmeier, H. Wang, M. Wiznitzer, K. Gurtz, A. Verganelaki, et al. 2004. Infantile-onset symptomatic epilepsy syndrome caused by a homozygous loss-of-function mutation of GM3 synthase. *Nat. Genet.* **36**: 1225–1229.
- Panzetta, P., H. J. Maccioni, and R. Caputto. 1980. Synthesis of retinal gangliosides during chick embryonic development. *J. Neurochem.* **35**: 100–108.
- Denny, C. A., J. Alroy, B. S. Pawlyk, M. A. Sandberg, A. d'Azzo, and T. N. Seyfried. 2007. Neurochemical, morphological, and neurophysiological abnormalities in retinas of Sandhoff and GM1 gangliosidosis mice. *J. Neurochem.* **101**: 1294–1302.
- Sango, K., S. Yamanaka, K. Ajiki, N. Arai, and M. Takano. 2008. Involvement of retinal neurons and pigment epithelial cells in a murine model of Sandhoff disease. *Ophthalmic Res.* **40**: 241–248.
- Mohand-Said, S., M. Weber, D. Hicks, H. Dreyfus, and J. A. Sahel. 1997. Intravitreal injection of ganglioside GM1 after ischemia reduces retinal damage in rats. *Stroke*. **28**: 617–621, discussion 622.
- Choi, J. S., J. A. Kim, and C. K. Joo. 2003. Activation of MAPK and CREB by GM1 induces survival of RGCs in the retina with axotomized nerve. *Invest. Ophthalmol. Vis. Sci.* **44**: 1747–1752.
- Wagener, R., B. Kobbe, and W. Stoffel. 1996. Quantification of gangliosides by microbore high performance liquid chromatography. *J. Lipid Res.* **37**: 1823–1829.
- Neville, D. C., V. Coquard, D. A. Priestman, D. J. te Vruchte, D. J. Sillence, R. A. Dwek, F. M. Platt, and T. D. Butters. 2004. Analysis of fluorescently labeled glycosphingolipid-derived oligosaccharides following ceramide glycanase digestion and anthranilic acid labeling. *Anal. Biochem.* **331**: 275–282.
- Farwanah, H., and T. Kolter. 2012. Lipidomics of glycosphingolipids. *Metabolites*. **2**: 134–164.
- Merrill, A. H., Jr., M. C. Sullards, J. C. Allegood, S. Kelly, and E. Wang. 2005. Sphingolipidomics: high-throughput, structure-specific, and quantitative analysis of sphingolipids by liquid chromatography tandem mass spectrometry. *Methods*. **36**: 207–224.

24. Merrill, A. H., Jr. 2011. Sphingolipid and glycosphingolipid metabolic pathways in the era of sphingolipidomics. *Chem. Rev.* **111**: 6387–6422.
25. Svennerholm, L. 1957. Quantitative estimation of sialic acids. II. A colorimetric resorcinol-hydrochloric acid method. *Biochim. Biophys. Acta.* **24**: 604–611.
26. Dreyfus, H., B. Guerold, L. Freysz, and D. Hicks. 1997. Successive isolation and separation of the major lipid fractions including gangliosides from single biological samples. *Anal. Biochem.* **249**: 67–78.
27. Edel-Harth, S., H. Dreyfus, P. Bosch, G. Rebel, P. F. Urban, and P. Mandel. 1973. Gangliosides of whole retina and rod outer segments. *FEBS Lett.* **35**: 284–288.
28. Fontaine, V., D. Hicks, and H. Dreyfus. 1998. Changes in ganglioside composition of photoreceptors during postnatal maturation of the rat retina. *Glycobiology.* **8**: 183–190.
29. Gazzotti, G., S. Sonnino, and R. Ghidoni. 1985. Normal-phase high-performance liquid chromatographic separation of nonderivatized ganglioside mixtures. *J. Chromatogr.* **348**: 371–378.
30. Ikeda, K., and R. Taguchi. 2010. Highly sensitive localization analysis of gangliosides and sulfatides including structural isomers in mouse cerebellum sections by combination of laser microdissection and hydrophilic interaction liquid chromatography/electrospray ionization mass spectrometry with theoretically expanded multiple reaction monitoring. *Rapid Commun. Mass Spectrom.* **24**: 2957–2965.
31. Lydic, T. A., J. V. Busik, and G. E. Reid. 2014. A monophasic extraction strategy for the simultaneous lipidome analysis of polar and nonpolar retina lipids. *J. Lipid Res.* **55**: 1797–1809.
32. Holm, M., and J. E. Mansson. 1974. Differences in sphingosine and fatty acid patterns of the major gangliosides of bovine retina. *FEBS Lett.* **38**: 261–262.
33. Fliesler, S. J., and R. E. Anderson. 1983. Chemistry and metabolism of lipids in the vertebrate retina. *Prog. Lipid Res.* **22**: 79–131.
34. Daniotti, J. L., C. A. Landa, and H. J. Maccioni. 1994. Regulation of ganglioside composition and synthesis is different in developing chick retinal pigment epithelium and neural retina. *J. Neurochem.* **62**: 1131–1136.
35. Tsui, Z. C., Q. R. Chen, M. J. Thomas, M. Samuel, and Z. Cui. 2005. A method for profiling gangliosides in animal tissues using electrospray ionization-tandem mass spectrometry. *Anal. Biochem.* **341**: 251–258.
36. Huang, Q., X. Zhou, D. Liu, B. Xin, K. Cechner, H. Wang, and A. Zhou. 2014. A new liquid chromatography/tandem mass spectrometry method for quantification of gangliosides in human plasma. *Anal. Biochem.* **455**: 26–34.
37. Svennerholm, L., and P. Fredman. 1980. A procedure for the quantitative isolation of brain gangliosides. *Biochim. Biophys. Acta.* **617**: 97–109.
38. Ikeda, K., T. Shimizu, and R. Taguchi. 2008. Targeted analysis of ganglioside and sulfatide molecular species by LC/ESI-MS/MS with theoretically expanded multiple reaction monitoring. *J. Lipid Res.* **49**: 2678–2689.
39. Hidari, K., S. Itonori, Y. Sanai, M. Ohashi, T. Kasama, and Y. Nagai. 1991. Isolation and characterization of a monosialosylgangliopentaosyl ceramide from *Xenopus laevis* oocyte. *J. Biochem.* **110**: 412–416.
40. Zhu, J., Y. T. Li, S. C. Li, and R. B. Cole. 1999. Structural characterization of gangliosides isolated from mullet milt using electrospray ionization-tandem mass spectrometry. *Glycobiology.* **9**: 985–993.
41. Lingwood, D., and K. Simons. 2010. Lipid rafts as a membrane-organizing principle. *Science.* **327**: 46–50.
42. Hakomori, S. I. 2002. The glycosynapse. *Proc. Natl. Acad. Sci. USA.* **99**: 225–232.
43. Todeschini, A. R., J. N. Dos Santos, K. Handa, and S. I. Hakomori. 2008. Ganglioside GM2/GM3 complex affixed on silica nanospheres strongly inhibits cell motility through CD82/cMet-mediated pathway. *Proc. Natl. Acad. Sci. USA.* **105**: 1925–1930.
44. Fong, B., C. Norris, E. Lowe, and P. McJarow. 2009. Liquid chromatography-high-resolution mass spectrometry for quantitative analysis of gangliosides. *Lipids.* **44**: 867–874.
45. Garcia, A. D., J. L. Chavez, and Y. Mechref. 2014. Rapid and sensitive LC-ESI-MS of gangliosides. *J. Chromatogr. B Analyt. Technol. Biomed. Life Sci.* **947–948**: 1–7.
46. Giuffrida, F., I. M. Elmelegy, S. K. Thakkar, C. Marmet, and F. Destailats. 2014. Longitudinal evolution of the concentration of gangliosides GM3 and GD3 in human milk. *Lipids.* **49**: 997–1004.
47. Fuller, M., S. Duplock, L. K. Hein, B. A. Rigat, and D. J. Mahuran. 2014. Liquid chromatography/electrospray ionisation-tandem mass spectrometry quantification of GM2 gangliosides in human peripheral cells and plasma. *Anal. Biochem.* **458**: 20–26.
48. Gantner, M., G. Schwarzmann, K. Sandhoff, and T. Kolter. 2014. Partial synthesis of ganglioside and lysoganglioside lipofoms as internal standards for MS quantification. *J. Lipid Res.* **55**: 2692–2704.
49. Svennerholm, L. 1980. Ganglioside designation. *Adv. Exp. Med. Biol.* **125**: 11.
50. Schnaar, R. L., A. Suzuki, and P. Stanley. 2009. Glycosphingolipids. In *Essentials of Glycobiology*. A. Varki, R. D. Cummings, J. D. Esko, H. H. Freeze, P. Stanley, C. R. Bertozzi, G. W. Hart, and M. E. Etzler, editors. Cold Spring Harbor Laboratory Press, Cold Spring Harbor, NY.